II International Conference on Particle-based Methods - Fundamentals and Applications
PARTICLES 2011
E. Oñate and D.R.J. Owen (Eds)

ENRICHED CONVECTED PARTICLE DOMAIN INTERPOLATION (CPDI) METHOD FOR ANALYZING WEAK DISCONTINUITIES

ALIREZA SADEGHIRAD*, REBECCA M. BRANNON* AND JAMES GUILKEY†

*Department of Mechanical Engineering
University of Utah
50 S. Central Campus Dr., Salt Lake City, UT 84108, USA
e-mail: alireza.sadeghirad@utah.edu and rebecca.brannon@utah.edu
web page: http://www.mech.utah.edu/brannon/

†Schlumberger Technology Corporation
14910 Airline Road, Rosharon, TX 77583, USA
e-mail: james.guilkey@utah.edu
Web page: http://www.mech.utah.edu/people/faculty/guilkey.html

Key words: Convected Particle Domain Interpolation, Material Point Method, Enrichment Techniques, Weak Discontinuities.

Abstract. Convected particle domain interpolation (CPDI) is a recently developed technique for more accurately approximating material point method (MPM) integrals by replacing the shape functions with interpolations of the shape functions to corners of particle domains that are tracked as parallelograms in 2-D (or parallelepipeds in 3-D). In this paper, the CPDI method is enhanced to (1) more accurately track particle domains with very little computational overhead in comparison to the original CPDI, (2) remove gaps/overlapping between particle domains, and (3) give more flexibility in choosing particle domain shape in the initial configuration. This enhanced CPDI method is then enriched to accurately solve weak discontinuities in the displacement field across a material interface that passes through the interior of a grid cell. The new enriched CPDI2 method is demonstrated using one- and two-dimensional examples.

1 INTRODUCTION

The Material Point Method (MPM) [1, 2] and the closely related Generalized Interpolation Material Point (GIMP) method [3] have been successfully used in simulation of some complicated engineering problems (see for example [4, 5, 6, 7, 8, 9]). Like many other particle methods, both MPM and GIMP gain computational efficiency by solving

the governing equations on a background grid that can be retained or reset at the end of each time step, while field data are stored at moving Lagrangian particles. The conventional MPM, which considers each particle as a lumped mass, is well known to suffer from a "cell crossing instability" in large deformation problems caused by a jump discontinuity in the gradient of low-order shape functions across cell boundaries. The GIMP method eliminates this error by replacing point evaluation of the MPM integrals with a weighted average of the integrand over a finite domain in the neighborhood of the particle.

The GIMP weight, or characteristic, function is typically chosen to be a "top-hat" function that is equal to unity within a finite domain centered around the particle, and zero elsewhere. The standard MPM formulation is exactly recovered when the choice of characteristic function is the Dirac delta function. For large deformation problems, the GIMP method gains accuracy if particle domains are allowed to deform with the material. Some early efforts to evolve particle domains with deformation only allowed rectangles (or cuboids in 3-D) to change dimension but not shape. However, a first-order accurate description of domain convection must allow rectangles to deform to parallelograms (parallepipeds in 3-D) [10]. With a conventional GIMP formulation using a top-hat function, tracking particle domains as parallelograms is prohibitively costly because of a need to divide these parallelograms over cell boundaries to account for the changes in the shape functions across cell boundaries. The convected particle domain interpolation (CPDI) method [10] circumvents this problem by replacing the grid shape function with an alternative function that is an interpolation of the original shape function to the corners of the particle domain. Since the CPDI alternative shape function is smoothly varying over the particle domain, the revised MPM integrals may be evaluated analytically. In the original CPDI method, now called CPDI1, the particle domains were approximated to be parallelograms (or parallelepipeds in 3-D). An enhancement, called CPDI2, describes particle domains by quadrilaterals (or hexahedra in 3-D). Advantages of CPDI2 over CPDI1 include (1) more accurately tracking particle domains with very little computational overhead in comparison to CPDI1, (2) removing gaps/overlapping between particle domains, and (3) giving more flexibility in choosing particle domain shape in the initial configuration. Like CPDI1, the CPDI2 method describes fields over particle domains based on values of those fields mapped to the particle domain's corners.

In the MPM techniques, spurious non-monotonic variation in stress can occur at material interfaces passing through the interior of a grid cell. This problem is caused by low-order shape functions being incapable of describing the jump in displacement gradients needed to allow the compliant materials to experience larger strain than stiff material in the same cell. The CPDI2 method can rectify this shortcoming by supplementing the nodal degrees of freedom already defined on the background grid with the corner values of the fields at particles near a material interface. This approach provides enrichment capable of properly describing weak discontinuities in the displacement field (i.e., strong discontinuities in strain) across a material interface that passes through the interior of a grid cell. For clarity, this approach will be first demonstrated in a simple 1-D context,

where spurious stress spikes and dips caused by incorrect partitioning of deformation within a cell are eliminated through CPDI2 enrichment, thus giving results comparable to a traditional Lagrangian finite-element simulation that has a node at the material interface. Recognizing that particle methods are adopted in situations for which traditional Lagrangian finite elements or Eulerian finite difference methods are unsatisfactory, improvements in accuracy of CPDI2 over CPDI1, and even more dramatic improvements in comparison to legacy methods of evaluating non-advecting GIMP integrals, are presented.

The paper is organized as follows: Section (2) introduces the basic strategy of the material point methods. Section (3) presents the enhanced version of the original CPDI method. The enrichment technique for this enhanced version is explained in Section (4), followed by the numerical examples in Section (5). Finally, Section (6) draws some conclusion remarks.

2 REVIEW OF THE MPM TECHNIQUES

In this section, formulations of the conventional MPM, GIMP, and CPDI methods are presented based on the "update stress last (USL)" algorithm described by Bardenhagen [11]. In the MPM, particle mass and momentum are mapped to the grid nodes at the first of each time step.

$$m_i = \sum_p \varphi_{ip} m_p \tag{1}$$

$$\boldsymbol{v}_i = \frac{\sum_p \varphi_{ip} m_p \boldsymbol{v}_p}{m_i} \tag{2}$$

in which m_i and $\boldsymbol{v}_i$ are mass and velocity at grid node i, m_p and $\boldsymbol{v}_p$ are mass and velocity at particle p, and φ_{ip} can be viewed as the average of the i^{th} grid shape function, S_i, over the p^{th} particle,

$$\varphi_{ip} = \frac{1}{V_p^*} \int_{\Omega_\chi} \chi_p(\boldsymbol{x} - \boldsymbol{x}_p) S_i^*(\boldsymbol{x}) d\boldsymbol{x} \tag{3}$$

in which $\chi_p(\boldsymbol{x})$ and Ω_χ are the particle characteristic function and its support-domain of volume V_p^* respectively, and S_i^* is the shape function or, for CPDI, the alternative shape function. In the MPM, the characteristic function is chosen as the Dirac delta function and a "top-hat" characteristic function is typically used in the GIMP method:

$$\chi_p(\boldsymbol{x}) = \begin{cases} 1 & \boldsymbol{x} \in \Omega_\chi \\ 0 & \text{otherwise} \end{cases} \tag{4}$$

Whereas Ω_χ has been selected to be rectangular (or cuboid in 3-D) in legacy GIMP formulations, CPDI formulations are well suited to taking Ω_χ to be a better approximation to the Voronoi cell Ω_p associated with the particle.

In the MPM, the discretized weak form of the equations of motion,

$$m_i \boldsymbol{a}_i = \boldsymbol{f}_i^{\text{int}} + \boldsymbol{f}_i^{\text{ext}} \tag{5}$$

is solved at each time step. Here,

$$\boldsymbol{f}_i^{\text{int}} = -\int_\Omega \nabla S_i \cdot \boldsymbol{\sigma} d\Omega, \tag{6}$$

and

$$\boldsymbol{f}_i^{\text{ext}} = \int_\Omega \rho S_i \boldsymbol{b} d\Omega + \int_{\Gamma^t} S_i \boldsymbol{\tau} d\Gamma, \tag{7}$$

in which ∇S_i is the grid shape function gradient, $\boldsymbol{b}$ is the body force per unit mass, and Γ^t is the part of the problem domain boundary where the prescribed traction τ is applied.

The integral in Eq. (6) is broken into the sum of integrals over elements in the FEM, whereas the MPM breaks the integral over particle domains as

$$\boldsymbol{f}_i^{\text{int}} = -\sum_p \int_{\Omega_p} \nabla S_i \cdot \boldsymbol{\sigma} dV. \tag{8}$$

The stress over each particle domain is assumed to be approximately constant because particle domains are often small and variation of stress over them is negligible in comparison to variation of shape function gradients. In this case, the nodal internal forces can be calculated as

$$\boldsymbol{f}_i^{\text{int}} = -\sum_p \nabla \varphi_{ip} \cdot \boldsymbol{\sigma}_p V_p, \tag{9}$$

in which $\boldsymbol{\sigma}_p$ is the stress over the p^{th} particle domain, and

$$\nabla \varphi_{ip} = \frac{1}{V_p^*} \int_{\Omega_\chi} \chi_p(\boldsymbol{x} - \boldsymbol{x}_p) \nabla S_i^*(\boldsymbol{x}) d\boldsymbol{x}. \tag{10}$$

At each time step, grid node accelerations, grid node velocities, particle velocities, and particle positions are calculated as follows:

$$\boldsymbol{a}_i = \frac{\boldsymbol{f}_i^{\text{int}} + \boldsymbol{f}_i^{\text{ext}}}{m_i} \tag{11}$$

$$\boldsymbol{v}_i^{n+1} = \boldsymbol{v}_i^n + \boldsymbol{a}_i \Delta t \tag{12}$$

$$\boldsymbol{v}_p^{n+1} = \boldsymbol{v}_p^n + \sum_i \varphi_{ip} \boldsymbol{a}_i \Delta t \tag{13}$$

$$\boldsymbol{x}_p^{n+1} = \boldsymbol{x}_p^n + \sum_i \varphi_{ip} \boldsymbol{v}_i^{n+1} \Delta t \tag{14}$$

The velocity gradient at particles is computed by

$$\nabla \boldsymbol{v}_p^{n+1} = \sum_i \nabla \varphi_{ip} \boldsymbol{v}_i^{n+1} \tag{15}$$

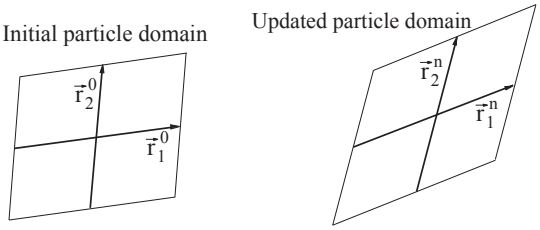

Figure 1: Initial and updated particle domain in the CPDI method.

Similarly, other kinematical quantities (such as the deformation gradient) are mapped to particles so that the particle stress tensor can be updated to the end of the time step by calling the constitutive model.

The conventional MPM considers each particle as a lumped mass, and there is no need to track particle domains in this method. For the GIMP method, two strategies are considered to track evolving particle domains under large deformations: uGIMP and cpGIMP. In the uGIMP, deformation of the particle domain is neglected and particle domains are tracked as fixed rectangles. In the cpGIMP, the particle sizes evolve based on only diagonal components of the deformation gradient at the particle so the particle domains remain rectangular. In the CPDI1 method, the updated particle domain at time step n is determined using the fully updated deformation gradient as

$$\begin{aligned} \boldsymbol{r}_1^n &= \boldsymbol{F}_p^n \boldsymbol{r}_1^0 \\ \boldsymbol{r}_2^n &= \boldsymbol{F}_p^n \boldsymbol{r}_2^0 \end{aligned} \tag{16}$$

where $(\boldsymbol{r}_1^0, \boldsymbol{r}_2^0)$ and $(\boldsymbol{r}_1^n, \boldsymbol{r}_2^n)$ are shown in Fig. 1. The following alternative grid shape functions are used in the CPDI method to efficiently calculate the integrals in Eq. (3) and Eq. (10) without incurring the expense of dividing the particle domains along cell boundaries:

$$S_i^*(\boldsymbol{x}) = \sum_{\alpha=1}^{4} N_\alpha^p(\boldsymbol{x}) S_i(\boldsymbol{x}_\alpha^p) \;\; \texttt{on} \;\; \Omega_p. \tag{17}$$

Here, N_α^p is the finite element shape function defined on the particle domain as a 4-node element. This shape function is defined for the α^{th} corner of the particle domain and $\boldsymbol{x}_\alpha^p$ is the position of this corner. Using the alternative grid shape functions, Eq. (3) and Eq. (10) can be written as

$$\begin{aligned} \varphi_{ip} &= \frac{1}{V_p} \int_{\Omega_p} S_i^*(\boldsymbol{x}) d\boldsymbol{x} = \frac{1}{V_p} \sum_{\alpha=1}^{4} \left(\int_{\Omega_p} N_\alpha^p(\boldsymbol{x}) d\boldsymbol{x} \right) S_i(\boldsymbol{x}_\alpha^p) \\ &= \frac{1}{4} \left\{ S_i(\boldsymbol{x}_1^p) + S_i(\boldsymbol{x}_2^p) + S_i(\boldsymbol{x}_3^p) + S_i(\boldsymbol{x}_4^p) \right) \} \end{aligned} \tag{18}$$

$$\nabla\varphi_{ip} = \frac{1}{V_p}\int_{\Omega_p}\nabla S_i^*(\boldsymbol{x})d\boldsymbol{x} = \frac{1}{V_p}\sum_{\alpha=1}^{4}\left(\int_{\Omega_p}\nabla N_\alpha^p(\boldsymbol{x})d\boldsymbol{x}\right)S_i(\boldsymbol{x}_\alpha^p)$$

$$= \frac{1}{2V_p}\left\{(S_i(\boldsymbol{x}_1^p)-S_i(\boldsymbol{x}_3^p))\begin{bmatrix} r_{1y}^n - r_{2y}^n \\ r_{2x}^n - r_{1x}^n \end{bmatrix} + (S_i(\boldsymbol{x}_2^p)-S_i(\boldsymbol{x}_4^p))\begin{bmatrix} r_{1y}^n + r_{2y}^n \\ -r_{1x}^n - r_{2x}^n \end{bmatrix}\right\} \quad (19)$$

Superiority of stability and accuracy of the CPDI1 solutions in comparison with the conventional MPM and GIMP solutions have been shown in [10].

3 THE CPDI2 METHOD

The original CPDI1 method tracks particle domains as parallelograms. The CPDI2 method, presented here, evolves particle domains as quadrilaterals. Specifically, particle domain corners are tracked instead of the particle centroid. When needed, the particle centroid $\boldsymbol{x}_p$ is determined based on the corner positions using the following equation:

$$\boldsymbol{x}_p = \frac{\boldsymbol{x}_1^p + \boldsymbol{x}_2^p + \boldsymbol{x}_3^p + \boldsymbol{x}_4^p}{4}, \quad (20)$$

where $\boldsymbol{x}_1^p$, $\boldsymbol{x}_2^p$, $\boldsymbol{x}_3^p$, and $\boldsymbol{x}_4^p$ are positions of four corners of the domain of particle p. The immediate conclusion is that there is no gap/overlapping between particle domains in the CPDI2 method. These particle domains are similar to a finite element mesh constructed using 4-node elements. Based on this algorithm, the particle domains are tracked as quadrilaterals. Similar to the CPDI1 formulation, using Eq. (17) as the alternative grid shape functions in the CPDI2 method, Eq. (3) and Eq. (10) can be written as

$$\varphi_{ip} = \frac{1}{V_p}\int_{\Omega_p} S_i^*(\boldsymbol{x})d\boldsymbol{x} = \frac{1}{V_p}\sum_{\alpha=1}^{4}\left(\int_{\Omega_p} N_\alpha^p(\boldsymbol{x})d\boldsymbol{x}\right)S_i(\boldsymbol{x}_\alpha^p)$$

$$= \frac{1}{4}\left\{S_i(\boldsymbol{x}_1^p)+S_i(\boldsymbol{x}_2^p)+S_i(\boldsymbol{x}_3^p)+S_i(\boldsymbol{x}_4^p))\right\} \quad (21)$$

$$\nabla\varphi_{ip} = \frac{1}{V_p}\int_{\Omega_p}\nabla S_i^*(\boldsymbol{x})d\boldsymbol{x} = \frac{1}{V_p}\sum_{\alpha=1}^{4}\left(\int_{\Omega_p}\nabla N_\alpha^p(\boldsymbol{x})d\boldsymbol{x}\right)S_i(\boldsymbol{x}_\alpha^p)$$

$$= \frac{1}{\beta_{1x}\beta_{2y}-\beta_{1y}\beta_{2x}}\left\{S_i(\boldsymbol{x}_1^p))\begin{bmatrix} -\beta_{2y}+\beta_{1y} \\ \beta_{2x}-\beta_{1x} \end{bmatrix} + S_i(\boldsymbol{x}_2^p)\begin{bmatrix} \beta_{2y}+\beta_{1y} \\ -\beta_{2x}-\beta_{1x} \end{bmatrix}\right.$$
$$\left. + S_i(\boldsymbol{x}_3^p)\begin{bmatrix} \beta_{2y}-\beta_{1y} \\ -\beta_{2x}+\beta_{1x} \end{bmatrix} + S_i(\boldsymbol{x}_4^p)\begin{bmatrix} -\beta_{2y}-\beta_{1y} \\ \beta_{2x}+\beta_{1x} \end{bmatrix}\right\} \quad (22)$$

in which (β_{1x},β_{1y}) and (β_{2x},β_{2y}) are respectively the components of vectors $\boldsymbol{\beta}_1 = -\boldsymbol{x}_1^p + \boldsymbol{x}_2^p + \boldsymbol{x}_3^p - \boldsymbol{x}_4^p$ and $\boldsymbol{\beta}_2 = -\boldsymbol{x}_1^p - \boldsymbol{x}_2^p + \boldsymbol{x}_3^p + \boldsymbol{x}_4^p$.

A major advantage of the CPDI2 method in comparison with the conventional finite element method is that the CPDI2 method enforces no-slip contact between bodies automatically without any further computational costs.

4 ENRICHMENT FOR THE CPDI2 METHOD

As will be shown in the numerical simulations in the next section, spurious non-monotonic variation in stress can occur at material interfaces passing through the interior of a grid cell in the MPM techniques. This problem is caused by low-order shape functions being incapable of describing the jump in displacement gradients needed to allow the compliant materials within the cell to deform more than stiff materials. In this section, an enriched version of the CPDI2 method is presented to accurately model the material interfaces passing through the interior of a grid cell.

Conceptually, the CPDI2 begins an analysis step by mapping data from particles to the particle corners. This step is embedded in the final expression (Eq. (21)) which maps directly from particles to grid nodes to solve the equations of motion (EOMs) on the grid. Eq. (21) can be rewritten as

$$\varphi_{ip} = \frac{1}{V_p} \sum_{\alpha=1}^{4} \left(\int_{\Omega_p} N_\alpha^p(\boldsymbol{x}) d\boldsymbol{x} \right) S_i(\boldsymbol{x}_\alpha^p) = \sum_{\alpha=1}^{4} R_\alpha^p S_i(\boldsymbol{x}_\alpha^p) \tag{23}$$

in which

$$R_\alpha^p = \frac{1}{V_p} \int_{\Omega_p} N_\alpha^p(\boldsymbol{x}) d\boldsymbol{x} \tag{24}$$

In this equation, R_α^p can be interpreted as the mapping function between particle p and particle corner α, and $S_i(\boldsymbol{x}_\alpha^p)$ can be considered as the mapping function between particle corner α and grid node i. If the algorithm were to map only to the corner nodes, then the resulting solution would be equivalent to an FEM solution. If the algorithm maps from corners to grid, then the resulting solution is the CPDI material point method. The particle domains in the CPDI2 are similar to 4-node finite element (Q4) with single point integration (particle corners and particles are analogous to FE nodes and Gauss points respectively).

To enrich the CPDI2 method, the nodal degrees of freedom already defined on the background grid can be supplemented with the corner values of the fields at the particles that are known to be near a material interface. This approach provides enrichment capable of properly describing weak discontinuities in the displacement field (i.e., strong discontinuities in strain) across a material interface that passes through the interior of a grid cell. Enriched CPDI2 is a hybrid of the two methods in which the MPM solution is used away from surfaces of discontinuity while the solution near the interface is resolved using the FEM solution that treats the corner nodes as supplemental degrees of freedom.

The distinguishing feature of enriched CPDI2 is that the grid nodes are supplemented with the enriched corner nodes for particles adjacent to an interface. As is done in all MPM formulations, the enriched CPDI2 algorithm loops over particles to accumulate contributions to the grid node mass, velocity, internal forces, etc., as in Eq. (1), Eq. (2), and Eq. (9). As is done in an ordinary CPDI2 implementation, the contribution of a particle to a grid node is evaluated as a sum of contributions from that particle's corners.

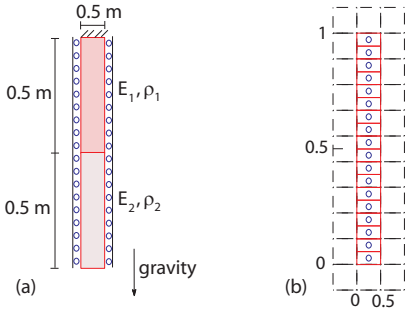

Figure 2: The vertical bi-material bar problem: (a) geometry and (b) discretized model.

In the loop over corners, non-enriched corners are treated the same as in a conventional CPDI formulation; namely,

$$\varphi_{ip} = \sum_{\beta} R^p_\beta \zeta_{i\beta p} \tag{25}$$

where

$$\zeta_{i\beta p} = \begin{cases} S_i(\boldsymbol{x}^p_\beta) & \text{if } \beta \text{ is not an enriched corner} \\ 1 & \text{otherwise} \end{cases} \tag{26}$$

5 NUMERICAL EXAMPLES

In this section, effectiveness of the enriched CPDI2 method is verified using numerical examples. The following Neo-Hookean material model is used in all numerical simulations.

$$\boldsymbol{\sigma} = \frac{\lambda \ln J}{J}\boldsymbol{I} + \frac{\mu}{J}(\boldsymbol{F}\boldsymbol{F}^T - \boldsymbol{I}) \tag{27}$$

in which $\boldsymbol{I}$ is the identity tensor, μ and λ are the shear modulus and Lam*é* constant respectively, $\boldsymbol{F}$ is the deformation gradient, and J is the determinant of $\boldsymbol{F}$.

5.1 Vibration of a bi-material bar under self weight

Vibration of a vertical bar under its own weight is considered in this example. The upper end of the bar is fixed, the right and left boundaries have roller boundary conditions, and the lower end is traction free as shown in Fig. 2a. The bar is composed of two parts with different elastic moduli: $E_1 = 2E_2 = 1 \times 10^7$Pa. Poisson's ratios and initial densities are $\nu_1 = \nu_2 = 0.3$ and $\rho^0_1 = \rho^0_2 = 1050\text{kg/m}^3$, respectively. Time steps are chosen as $\Delta t = 0.00005$s. Gravity, $g = -10\text{m/s}^2$, is applied suddenly as a step function at $t = 0$s. The initial problem domain is discretized by using 18 particles (2 per cell) as depicted in Fig. 2b. The material interface falls in the center of a grid cell.

Time histories of the displacement of particle A obtained from the GIMP, CPDI1, CPDI2, and enriched CPDI2 methods are presented in Fig. 3.

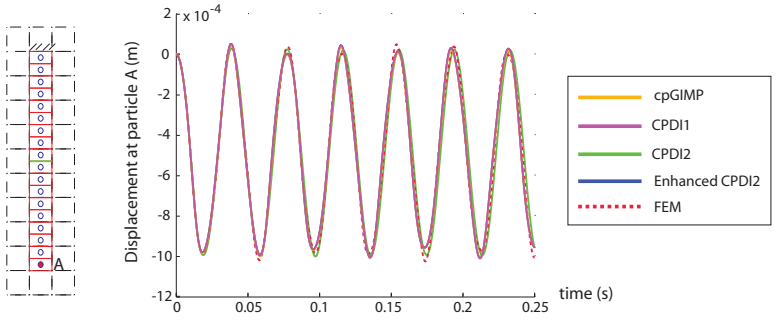

Figure 3: Time histories of the displacement of particle A in the bi-material bar under self weight simulations.

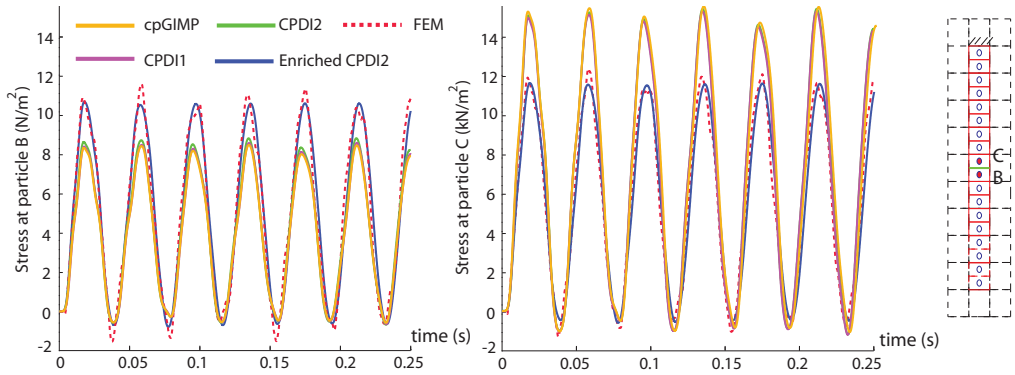

Figure 4: Time histories of the stresses of particles B and C in the bi-material bar under self weight simulations.

Without enrichment, a conventional MPM or CPDI solution to this problem exhibits a spuriously large stress in the stiff material and spuriously low stress in the compliant material. Fig. 4, which shows time histories of the stresses of particles B and C demonstrates that the enriched CPDI2 method improves the results by producing stresses at points B and C that are nearly equal to each other, as they should be. The stress profiles in Fig. 5 further illustrate the spurious non-monotonic variations in stress profiles near the material interfaces passing through the interior of a grid cell that are eliminated with enrichment.

5.2 Bi-material ring under centrifugal force

A bi-material ring under centrifugal force is simulated in this example. The ring is composed of two compliant and stiff rings as shown in Fig. 6. The following values are chosen for numerical simulations: modulus of elasticity $E_1 = 2E_2 = 1 \times 10^9$Pa, Poisson's ratios $\nu_1 = \nu_2 = 0.3$, initial densities $\rho_1^0 = \rho_2^0 = 1000\text{kg/m}^3$, inner radius $r_i = 3$m, outer radius $r_o = 3.2$m, and time step $\Delta t = 0.000001$s. Due to symmetry, only one-quarter of

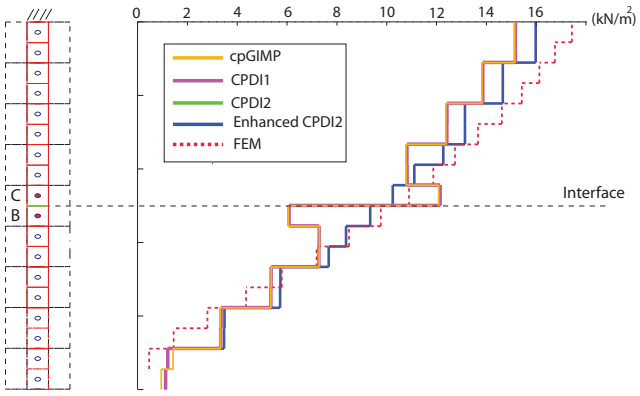

Figure 5: Stress profiles at $t = 0.14$s in the bi-material bar under self weight simulations.

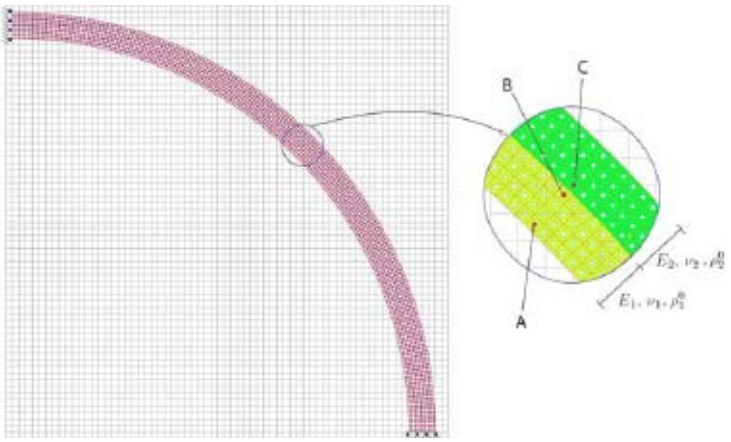

Figure 6: Initial configuration of four different resolutions used in modeling one-quarter of the ring.

the ring is modeled. The problem domain is discretized by using 1544 particles as shown in Fig. 6. The ring suddenly starts to rotate with a frequency of $\omega = 1$rad/s at $t = 0$. To capture the centrifugal force, the following body forces (per unit mass) are applied to the numerical model:

$$b_r = \omega^2 r \tag{28}$$

$$b_\theta = 0 \tag{29}$$

in which b is the body forces in the cylindrical coordinates, ρ is the density, and r and θ are cylindrical coordinates.

Fig. 7 depicts time histories of the displacement of particle A (located as shown in Fig. 6), showing that CPDI2, enriched CPDI2, and FEM all give similar results for displacement.

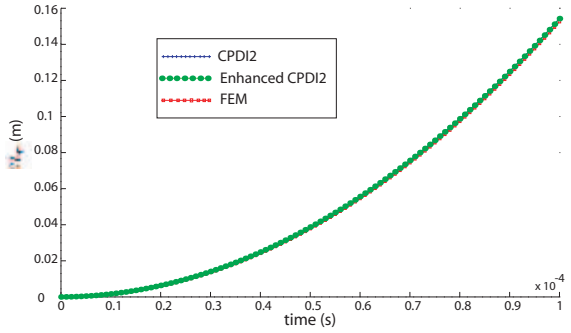

Figure 7: Time histories of the displacement of particle A in the bi-material ring under centrifugal force simulations.

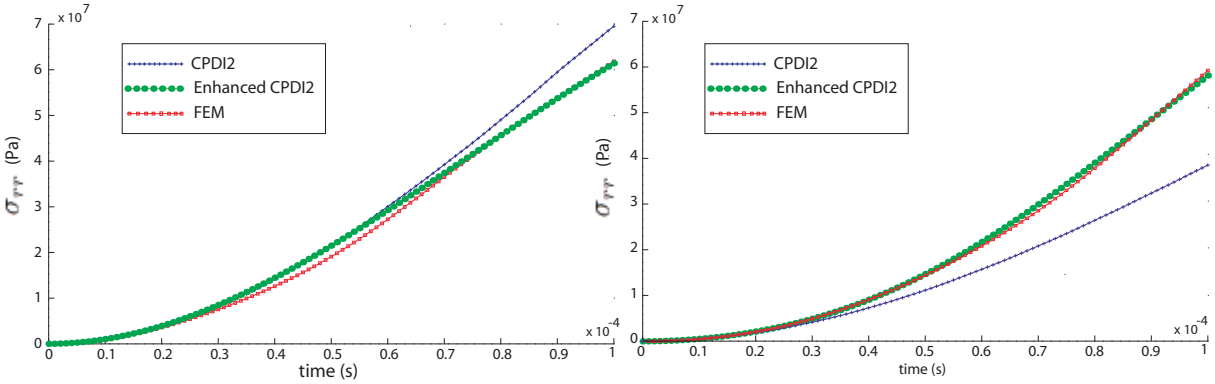

Figure 8: Time histories of the radial components of the stresses of particles B and C, respectively, in the bi-material ring under centrifugal force simulations.

Fig. 8 shows time histories of the radial components of the stresses of particles B and C. As shown in this figure, the CPDI2 method over predicts and under predicts stresses of particles B and C respectively. The enriched CPDI2 method leads to the similar stresses to the reference solution (i.e. the finite element solution).

6 CONCLUSIONS

An enhanced version of the convected particle domain interpolation (CPDI) method, named CPDI2, has been developed to further improve upon the accuracy of the original CPDI method by removing gaps/overlapping between particle domains without significantly impacting numerical efficiency. By modeling particle domains as quadrilaterals, the CPDI2 method not only offers greater flexibility in choosing particle domains shape in the initial configuration, but it also provides a natural computational framework for enrichment of fields though supplementing nodal degrees of freedom on the grid with the corner values of the fields at the particles near material interfaces. Accordingly, the

CPDI2 method has been demonstrated to be an efficient and accurate particle method in solving problems with weak discontinuities. As documented separately, the method also provides a natural means of enforcing boundary conditions. Future work will address strong discontinities, such as fractures.

REFERENCES

[1] Sulsky, D., Chen, A. and Schreyer, H. A particle method for history-dependent materials. *Comput. Meth. Appl. Mech. Eng.* (1994) **118**:179–196.

[2] Sulsky, D., Zhou, S. and Schreyer, H. Application of a particle-in-cell method to solid mechanics. *Comput. Phys. Commun.* (1995) **87**:236–252.

[3] Bardenhagen, S. and Kober, E. The generalized interpolation material point method. *Comput. Model. Eng. Sci.* (2004) **5**:477–495.

[4] York, A., Sulsky, D. and Schreyer, H. Fluid-membrane interaction based on the material point method. *Int. J. Num. Meth. Engng.* (2000) **48**:901–924.

[5] Bardenhagen, S., Guilkey, J., Roessig, K., Brackbill, J., Witzel, W. and Foster, J. An improved contact algorithm for the material point method and application to stress propagation in granular material. *Comput. Model. Eng. Sci.* (2001) **2**:509–522.

[6] Schreyer, H., Sulsky, D. and Zhou, S. Modeling delamination as a strong discontinuity with the material point method. *Comput. Meth. Appl. Mech. Eng.* (2002) **191**:2483–2507.

[7] Guo, Y. and Nairn, J. Three-dimensional dynamic fracture analysis using the material point method. *Comput. Model. Eng. Sci.* (2006) **16**:141–155.

[8] Daphalapurkar, N., Lu, H., Coker, D. and Komanduri, R. Simulation of dynamics crack growth using the generalized interpolation material point (gimp) method. *Int. J. Fract.* (2007) **143**:79–102.

[9] Zhang, H., Wang, K. and Chen, Z. Material point method for dynamic analysis of saturated porous media under external contact/impact of solid bodies. *Comput. Meth. Appl. Mech. Eng.* (2009) **198**:1456–1472.

[10] Sadeghirad, A., Brannon, R. and Burghardt, J. A convected particle domain interpolation technique to extend applicability of the material point method for problems involving massive deformations. *Int. J. Num. Meth. Engng.* (2011) **86**:1435–1456.

[11] Bardenhagen, S. Energy conservation error in the material point method for solid mechanics. *J. Comput. Phys.* (2002) **180**:383–403.